Impact of Gravity on the Bubble-to-Pulse Transition in Packed Beds

Paul Salgi and Vemuri Balakotaiah
Dept. of Chemical and Biomolecular Engineering, University of Houston, Houston TX 77204

DOI 10.1002/aic.14300
Published online December 19, 2013 in Wiley Online Library (wileyonlinelibrary.com)

A model based on two-phase volume-averaged equations of motion is proposed to examine the gravity dependence of the bubble-to-pulse transition in gas-liquid cocurrent down-flow through packed beds. As input, the model uses experimental correlations for the frictional pressure drop under both normal gravity conditions and in the limit of vanishing gravity, as well as correlations for the liquid-gas interfacial area per unit volume of bed in normal gravity. In accordance with experimental observations, the model shows that, for a given liquid flow, the transition to the pulse regime occurs at lower gas-flow rates as the gravity level or the Bond number is decreased. Predicted transition boundaries agree reasonably well with observations under both reduced and normal gravity. The model also predicts a decrease in frictional pressure drop and an increase in total liquid holdup with decreasing gravity levels. © 2013 American Institute of Chemical Engineers *AIChE J*, 60: 778–793, 2014
Keywords: gas-liquid flow, packed beds, reduced gravity, bubble-to-pulse transition, closure relations

Introduction

Due to their compactness, reliability, and relatively low power and maintenance requirements, packed bed reactors have been identified as a potential technology for use in support of long duration manned space missions.[1] Applications include *in situ* chemical processing and life-support operations such as wastewater treatment and air revitalization. Previous experiments[2] on the hydrodynamics of gas-liquid flow have shown that gravity affects both the nature of the flow regimes that are observed under fixed flow conditions and the transition boundaries between such regimes. In particular, under microgravity conditions (ca. ± 0.02 g), trickle flow is not observed in packed beds where gas and liquid are flowing cocurrently.[2] Instead, trickle flow is replaced with either bubble or pulse flow, depending on fluid/bed properties and flow conditions. When gas is introduced at a low rate, discrete bubbles are observed to form and flow in relatively straight lines. The bubbles undergo successive acceleration and deceleration as they squeeze through the narrow constrictions. This does not happen in a smooth, continuous fashion, as the bubbles seem to stop for a while in front of a constriction and then quickly squeeze through the constriction. On average, the size of the bubbles is small enough to allow for lateral "jumps" between neighboring channels (through lateral constrictions) without creating appreciable radial interaction between the channels. As the gas flow rate is increased, the following behavior is observed with increasing frequency in the axial flow channels: the bubbles tend to crowd in a file upstream of a plugged narrow constriction, then accelerate through the constriction in the form of a very long (several packing diameters), thin bubble (almost a "slug-annular" flow configuration at the pore level). These long bubbles travel through several constrictions without breaking-up and then seem to disintegrate back into smaller, slower moving bubbles after sudden decelaration (due perhaps to colliding with smaller bubbles or a packing sphere that blocks their flow path). As bed-level pulsing is approached by further increasing the gas flow rate, most of the flow in the axial channels is in the form of these long and thin bubbles, which seem to flow continuously without disintegrating, frequently crossing to neighboring channels by smoothly flowing over packing spheres. Motil et al.[2] defined the bubble-to-pulse "transition" as the gas flow rate at which the power-to-frequency ratio of the Fourier transformed pressure signal (from a point located near the center of the column) showed power concentrations of more than an order of magnitude at certain frequencies. The gas to liquid ratio at the transition was successfully correlated to a liquid Suratman number (ratio of the square of the Reynolds number to Weber number) as follows

$$\frac{G}{L}=0.02Su_l^{-0.15},\quad Su_l=\frac{\sigma d_p\rho_l}{\mu_l^2} \tag{1}$$

In the aforementioned equation, σ; is the surface tension at the gas-liquid interface, d_p is the packing size, and ρ_l and μ_l are the liquid density and shear viscosity, respectively. The quantities G and L are the gas and liquid mass flow rates per unit area of bed. Equation 1 correlates the data accurately for a wide range of liquid and gas flows as well as liquid viscosities.[3] The equation also accounts for data corresponding to two different values of the particle diameter (2 mm and 5 mm), although the Bond number ($Bo=\rho_l g(d_p)^2/\sigma$) based on the average gravity level is zero. However, Motil[3] found that,

Correspondence concerning this article should be addressed to P. Salgi at paslgi@central.uh.edu.

for normal gravity levels, the transition data at two different Bo values (corresponding to the two packing sizes) cannot be correlated with a single equation as in (1). Therefore, two additional correlations, similar to Eq. 1 were given to describe the data

$$\frac{G}{L}=\begin{cases}0.055Su_l^{-0.18} \text{ for } d_p=0.002 \text{ m } (Bo=0.54 \text{ for air/water})\\ 0.068Su_l^{-0.163} \text{ for } d_p=0.005 \text{ m } (Bo=3.36 \text{ for air/water})\end{cases} \quad (2)$$

It was also observed that, for a given liquid flow rate, the gas flow rate required for transitioning from bubble to pulse decreases with the Bond number. Motil[3] performed the normal gravity experiments with the gas and liquid flowing concurrently in the downward direction. No experimental data was obtained for the upward flow configuration.

Normal gravity studies of the bubble-to-pulse transition in gas-liquid cocurrent downward flow in packed beds are not as extensive as those related to the trickle-to-pulse transition because such columns are typically operated in the trickle to pulse region. We note the work of Boelhouwer et al.[4] who described flow regime transitions from trickle to pulse to dispersed bubble as the liquid superficial velocity is increased at fixed gas flow rate. They conclude that pulse flow is a sort of hybrid hydrodynamic regime where inter-pulse regions have flow patterns (liquid velocity and holdup) that are similar to those of trickle flow at the transition threshold (corresponding to the same superficial gas velocity), while pulse regions have characteristics similar to those of bubbly flow at the pulse-to-bubble transition corresponding to the same superficial gas velocity (e.g., higher liquid velocity and holdup.) These authors also note that as the pulse frequency increases with increasing liquid superficial velocity, the pulse regions merge into bubbly flow. Benkrid et al.[5] used a quasi-two-dimensional packed bed to visualize the motion of individual bubbles at very low-gas velocities. These authors observed large bubbles (compared to pore size) that undergo significant distortions as they flow through the network of pores. These bubbles were seen to get stuck in enlargements (being trapped by liquid bridges in the constrictions), oscillate for a few milliseconds, and then push through the liquid bridge ahead displacing it to the next constriction. Such behavior is consistent with the video observations of Motil et al.[2,3] at low-gas flow rates (under both micro and normal gravity conditions). A number of other experimental/modeling studies are also available in the literature on liquid holdup, pressure drop, and specific interfacial area in normal gravity bubbly flow.[6–10]

Many articles are available in the literature on the modeling of the trickle-pulse transition under normal gravity (see for instance Anadon et al.[11] for a brief review). These studies fall largely into two categories. In one group, the transition is modeled at the pore level as a result of instabilities in the liquid film surrounding the packing particles. In particular, we note the work of Ng[12] who obtains a transition criterion by writing an energy balance between the entrance and center of a constriction in the pore space separating two packing spheres, at the moment when the two neighboring liquid films are about to collapse. Holub et al.[13] have also developed a transition criterion by using Kapitza's criterion for the loss of laminar stability in liquid films. Another group of models[14–17] attempt to predict the trickle-to-pulse transition as a flow instability at the bed level. The volume-averaged separated two-phase flow equations are used to describe the flow. Stability of a base (uniform) state with respect to small perturbations is then analyzed by linearizing the flow equations, writing the velocity perturbations in terms of the liquid saturation perturbation with the help of the continuity equations, and substituting into a linear combination of the momentum equations to produce a single equation for the liquid saturation perturbation. Normal mode solutions to the initial value problem are then assumed and the eigenvalues of the characteristic equation are determined as a function of the physical parameters and the mode wave number and angular frequency. When flow conditions are such that the real parts of all eigenvalues are negative, the base flow is said to be stable. This flow becomes unstable for flow rate conditions under which the first real part of an eigenvalue crosses zero. Loss of stability in these models should signal the appearance of time-dependent flow at the length scales described by the models, which are typically larger than the pore size. This type of analysis treats the gas phase as incompressible and does not address the effect of column length or the location of the point of pulse inception. The base state is assumed to be homogeneous and loss of stability is typically the result of an increase of the average capillary pressure as the liquid holdup is decreased. Moreover, since this type of analysis is based on volume-averaged quantities, it does not give any information on the mechanisms underlying pore-level pulse formation or the evolution of such localized pulses to bed-size pulses. Notwithstanding the aforementioned limitations, we show in this article that this approach can be used to explain the main observations made by Motil et al.[2,3] regarding the impact of gravity on the bubble-to-pulse transition. Also, good quantitative agreement with bubble-to-pulse transition data is obtained across gravity levels.

Model Assumptions and Equations

Volume-averaged two-phase flow equations assume the existence of an intermediate length scale (the "mesoscale"), which is much larger than the size of the heterogeneities (e.g., pores or bubbles), and much smaller than the size of the overall system. In the case of a packed bed, we could picture a mesoscale volume element as having linear dimensions equivalent to several particle diameters. The size of the bubbles is also assumed to be large compared with the continuum scale so that the continuum field equations may be written and averaged. In the absence of material transfer at the interface, the averaged mass and momentum conservation equations for phase k (liquid or gas) at the mesoscale may be written formally as follows[18–20]

$$\frac{\partial \varepsilon_k \rho_k}{\partial t}+\nabla\cdot(\varepsilon_k\rho_k\vec{v}_k)=0 \quad (3)$$

$$\frac{\partial(\varepsilon_k\rho_k\vec{v}_k)}{\partial t}+\nabla\cdot(\varepsilon_k\rho_k\vec{v}_k\vec{v}_k)=-\varepsilon_k\nabla p_k+\nabla\cdot\left(\varepsilon_k\left(\boldsymbol{\tau}_k+\boldsymbol{\tau}_k^t\right)\right)+\varepsilon_k\rho_k g_k+\vec{M}_k \quad (4)$$

In these equations, ε_k is the time smoothed volume fraction of phase k at mesoscale ($\varepsilon_g+\varepsilon_l=1$.) The quantities ρ_k and p_k are the time smoothed phasic averages of the local (continuum scale) density and pressure of phase k. The velocity $\vec{v}_k$ is the time-smoothed, mass-weighted average of the local (continuum scale) velocity. The quantity $\boldsymbol{\tau}_k$ is the sum of two tensors, the "bulk" deformation stress tensor constructed using the mass-weighted phase averaged velocities,

and the interfacial "extra" deformation stress tensor which arises from the averaging of local velocity fluctuations at the interface. The term τ_k^I represents the time-smoothed, mass-weighted average of local velocity fluctuations. This term follows from the averaging of the momentum flux tensor but is usually grouped with the deformation stress tensor. In dispersed bubbly flow this term applies to the liquid phase and accounts for cofluctuations in the local (continuum) liquid velocity due to turbulence or the presence of bubbles. The term $\vec{M}_k$ is also a momentum transfer term and may be divided into two parts,[20,21] the Archimedes force due to the net action of the liquid acceleration and gravity, and the resultant force due to the relative motion of the two phases. In addition to Eqs. 3 and 4, formal averaging leads to so-called "jump conditions" for both mass and momentum. The mass jump condition is not relevant when, as is the case here, there is no material transfer (evaporation/condensation) at the interface. Assuming a uniform surface tension over the interface, the momentum jump condition[18,19] formally relates the sum of the momentum transfer terms of the two phases to the time smoothed, volume averaged mean curvature of the interface. The difficulty in applying Eqs. 3 and 4 to the description of a specific problem lies in the necessity of supplementing these equations with reasonable constitutive or closure relations for the various mesoscale variables. Because of the complexity of flow patterns in packed beds, the typical approach has been to use empirical correlations for the momentum transfer terms.[14] The bulk deformation stress tensor, the extra-deformation stress tensor, and the "Reynolds" tensor of the liquid phase at mesoscale are typically lumped into a single stress tensor of Newtonian form with an effective viscosity. In the gas phase, this tensor is neglected. The difference between interfacial and phasic averages of the pressure in phase k is also typically neglected in packed bed applications. This assumption, combined with the assumption of no material transfer and the neglect of the normal stress terms, leads to the following momentum jump condition[18]

$$p_g - p_l = 2H\sigma \tag{5}$$

where H is the mesoscale average value of the mean curvature of the interface. In linear stability studies of the trickle to pulse transition, this term plays an important role because it is the one that stabilizes the homogeneous flow. To model this "capillary" pressure term, Grosser et al.[14] used the Leverett J function corresponding to the drainage curve in a porous medium, which describes the variation in pressure difference as the liquid saturation is decreased, as in the case of a transition to pulsing that is approached from trickling flow by gradually increasing the gas flow rate. Attou and Ferschneider[16] used the momentum jump condition of Eq. 5 directly, wrote the mean curvature in terms of two principal radii of curvature at the pore scale, and obtained expressions for these two radii in terms of the gas volume fraction, the particle diameter and bed porosity. However, to obtain an expression that reproduces the trickle to pulse transition over a wide range of operating pressure, these authors had to multiply the term $2H\sigma$ by an empirical factor that accounts for gas density effects.

In this work, we propose a different approach which relates the capillary pressure to the interfacial area per unit volume. If the interfacial area per unit volume a_{int}, (which is accessible from mass-transfer experiments) is pictured as the area of an equivalent sphere of radius R, then it is easily shown that

$$H = \frac{1}{\mathrm{R}} = \frac{a_{int}(\varepsilon_l)}{3\varepsilon(1-\varepsilon_l)} \tag{6}$$

If the bubble size and shape vary significantly, as is the case in our problem, an additional factor may be included to account for deviations of the actual average value of surface area to volume from that obtained using a sphere of mean diameter.[18] Therefore, we write

$$H = C\frac{a_{int}(\varepsilon_l)}{3\varepsilon(1-\varepsilon_l)} \tag{6a}$$

In Eqs. 6 and 6a, ε represents the bed porosity. More details are given in a subsequent section on the determination of the prefactor C. For the specific interfacial area, we use Wild's et al.[22] correlation in the high-interaction regime. All flow conditions corresponding to the data of Motil et al.[2,3] do actually fall under this regime as defined by Wild et al. With the inclusion of the proper Bond number dependence in the factor C, the magnitude of the first derivative of H, as given by Eq. 6a, leads to a reasonably accurate prediction of the bubble-to-pulse transition under a wide range of flow properties and for various gravity levels.

The next set of required closure relations concerns the momentum transfer terms $\vec{M}_l$ and $\vec{M}_g$. As mentioned earlier, these terms may be written as the sum of two contributions, the Archimedes force and the net force due to the relative motion of the phases (which includes drag and non-drag contributions due to stress tensor fluctuations along the interface). For the liquid phase, this net force will in turn consist of two contributions, one due to the interaction of the liquid with the solid particles and another for the interaction of the liquid with the gas phase. In the case of a wetting liquid, the gas phase will only interact with the liquid. This leads to the following expressions for $\vec{M}_l$ and $\vec{M}_g$:

$$\vec{M}_l = -\rho_l\varepsilon_g\left(\frac{D\vec{v}_l}{dt} - \vec{g}\right) + \vec{f}_{sl} - \vec{f}_{lg} \tag{7}$$

$$\vec{M}_g = \rho_l\varepsilon_g\left(\frac{D\vec{v}_l}{dt} - \vec{g}\right) + \vec{f}_{lg} \tag{8}$$

In Eqs. 7 and 8, $\vec{f}_{sl}$ is the force exerted by the solid on the liquid per unit of void volume, and $\vec{f}_{lg}$ is the force exerted by the liquid on the gas per unit void volume. In packed bed applications, non-drag contributions are typically neglected, even though, in principle at least, added mass and memory effects should be included due to the strong accelerations and decelerations experienced by the bubbles.[23] In addition, as pointed out by Bordas et al.[23] the use of drag correlations obtained from data in open pipes cannot be justified for at least two reasons. First, the confinement factor due to the presence of the solid particles precludes the use of such correlations which are typically written as the product of the drag on a single particle in an "infinite" extent of liquid and a "hindering" factor that takes into account interactions between bubbles. As mentioned by these authors, such correlations hold for flows in channels whose size is much larger than the capillary length. Also, these drag correlations typically apply to nearly spherical bubbles, whereas in a packed bed, bubbles undergo significant deformation. Based on these considerations, we propose to use only correlations that are

relevant to packed beds in order to develop the required closure relations.

In the preceding paragraphs, we have written the equations in three-dimensional form but the radial dimensions of the lab-scale columns used by Motil et al.[2,3] to generate the data are of the order of the mesoscale length. Consequently, these equations may be considered as area averaged equations and the flow at mesoscale may be assumed to be (1-D) and in the (axial) direction of the flow. In what follows, we shall restrict the notation to 1-D flow with the reference direction pointing in the direction of flow.

Closure relation for $\vec{f}_{ls}=-\vec{f}_{sl}$

For the liquid–solid interaction we use a modified Ergun equation that accounts for the reduction in available void space for the liquid phase due to the presence of the gas phase[6,24]

$$f_{ls}=\frac{1}{\varepsilon_l^2}\left[\frac{180(1-\varepsilon)^2\mu_l}{\varepsilon^3 d_p^2}V_{sl}+\frac{1.8(1-\varepsilon)\rho_l}{\varepsilon^3 d_p}V_{sl}^2\right] \tag{9a}$$

For convenience of notation, we define

$$A_{ls}=\frac{180(1-\varepsilon)^2\mu_l}{\varepsilon^3 d_p^2}V_{sl}+\frac{1.8(1-\varepsilon)\rho_l}{\varepsilon^3 d_p}V_{sl}^2 \tag{9b}$$

In the aforementioned equation, V_{sl} and V_{sg} are the liquid and gas superficial velocities, ρ_l and μ_l are the density and viscosity of the liquid phase, d_p is the packing size, and ε is the bed porosity.

Closure relation for $\vec{f}_{gl}=-\vec{f}_{lg}$

In packed bed applications, the typical approach is to assume a base steady state with uniform velocities. Furthermore, the uniform mesoscale velocities are assumed equal to the traditional packed-bed "interstitial" velocities. As a result, the continuity equations are trivially satisfied in the base state and the two momentum equations are used to solve for the pressure drop and the liquid holdup, assuming an empirical form for both f_{ls} (see, for instance, Eq. 9a) and f_{lg}. These closed form expressions are usually of the Ergun type and display an explicit dependence on the liquid holdup and the relative velocity of the phases.[14–16] The validity of such expressions is then checked *a posteriori* based on the model prediction for the steady-state pressure drop and liquid holdup and for the flow-regime transition. This approach has yielded reasonable predictions for the trickle-pulse transition. However, Ergun type expressions for f_{gl} cannot be justified in the dispersed bubble flow regime and, as discussed in the previous section, expressions based on gas-liquid drag correlations in bubbly flow through open pipes cannot be used either. To avoid these difficulties, we propose the following approach.

In the uniform base state, the momentum conservation equations reduce to

$$-\varepsilon_l^0\frac{dp_0}{dx}-f_{ls}^0+f_{gl}^0+\rho_l g=0;\quad \text{Liquid} \tag{10}$$

$$-\left(1-\varepsilon_l^0\right)\frac{dp_0}{dx}-f_{gl}^0+\left(\rho_g-\rho_l\right)\left(1-\varepsilon_l^0\right)g=0;\ \text{Gas} \tag{11}$$

The steady-state pressure gradient (which is traditionally assumed to be the same in the liquid and gas phases) is written typically as the sum of a frictional pressure drop and a static head

$$-\frac{dp_l^0}{dx}=-\left.\frac{dp}{dx}\right]_{f_0}-\left[\varepsilon_l^0\rho_l+(1-\varepsilon_l^0)\rho_g\right]g \tag{12}$$

The following correlation for the frictional pressure drop in the limit of vanishing gravity was obtained by Motil et al.[2] and validated for a wide range of flow conditions (both bubble and pulse flow) and liquid viscosities

$$-\left.\frac{dp}{dx}\right]_{f_0}\left(\frac{d_p\varepsilon^3}{\rho_l V_{sl}^2(1-\varepsilon)}\right)=\frac{1}{\mathrm{Re}_l}\left[180+0.8(\mathrm{Re}_g)^{\frac{1}{2}}\left(\frac{Su_l}{\mathrm{Re}_l}\right)^{\frac{2}{3}}\right]+1.8 \tag{13}$$

The dimensionless numbers are given by

$$\mathrm{Re}_g=\frac{\rho_g V_{sg}d_p}{\mu_g(1-\varepsilon)}\quad \mathrm{Re}_l=\frac{\rho_l V_{sl}d_p}{\mu_l(1-\varepsilon)}\quad Su_l=\frac{\rho_l d_p\sigma}{\mu_l^2} \tag{14}$$

Since for a liquid flowing alone the frictional pressure drop is independent of gravity, it is the additional term due to the presence of the gas phase that must change with gravity. In dimensionless form, this term may be written as follows

$$\frac{-\left.\frac{dp}{dx}\right]_{f_0}^{\text{extra}}}{\sigma/d_p^2}=0.8\left(\frac{1-\varepsilon}{\varepsilon}\right)^3(\mathrm{Re}_g)^{\frac{1}{2}}\left(\frac{\mathrm{Re}_l}{Su_l}\right)^{\frac{1}{3}} \tag{15}$$

Equation 15 indicates that, under microgravity conditions, the ratio of the lefthand side to the group multiplying 0.8 on the righthand side is a constant (0.8) that is independent of bed properties and flow conditions. In the presence of gravity, we propose to write Eq. 15 in the more general form

$$\frac{-\left.\frac{dp}{dx}\right]_{f_0}^{\text{extra}}}{\sigma/d_p^2}=\alpha\left(\frac{1-\varepsilon}{\varepsilon}\right)^3(\mathrm{Re}_g)^{\frac{1}{2}}\left(\frac{\mathrm{Re}_l}{Su_l}\right)^{\frac{1}{3}} \tag{16}$$

In Eq.16, the parameter α will depend in general on the gravity level, flow orientation relative to gravity, and flow and bed conditions. This is equivalent to recasting frictional pressure drop correlations in a form similar to the one proposed by Motil et al.[2]

$$-\left.\frac{dp}{dx}\right]_{f_0}\left(\frac{d_p\varepsilon^3}{\rho_l V_{sl}^2(1-\varepsilon)}\right)=\frac{1}{\mathrm{Re}_l}\left[180+\alpha(\mathrm{Re}_g)^{\frac{1}{2}}\left(\frac{Su_l}{\mathrm{Re}_l}\right)^{\frac{2}{3}}\right]+1.8 \tag{17}$$

Under normal gravity conditions, expressions for the parameter α may be obtained from available frictional pressure drop correlations (Rao et al.[6], Khan et al.[25]). For concurrent downflow (Rao et al.[6]) we have

$$\alpha_1=\left[E_1\left(\mathrm{Re}_g\right)^{0.4}(\mathrm{Re}_l)^{0.05}-1.8\,\mathrm{Re}_l-180\right]\ \left(\mathrm{Re}_g\right)^{-0.5}\ \left(\frac{\mathrm{Re}_l}{Su_l}\right)^{\frac{2}{3}} \tag{18}$$

The constant E_1 is given by

$$E_1=2300(1-\varepsilon)^{-0.05}\varepsilon^{0.75}\left(\frac{\rho_l}{\rho_g}\right)\left(\frac{\mu_g}{\mu_l}\right)^2 \tag{18a}$$

For concurrent upflow (Khan et al.[25]) we have

$$\alpha_{-1}=\left[E_{-1}\left(\mathrm{Re}_g\right)^{0.18}\left(\mathrm{Re}_l\right)^{-0.7}-1.8\,\mathrm{Re}_l-180\right]\ \left(\mathrm{Re}_g\right)^{-0.5}\ \left(\frac{\mathrm{Re}_l}{Su_l}\right)^{\frac{2}{3}} \tag{19}$$

The constant E_{-1} is given by

$$E_{-1}=1.5\times10^{7}(1-\varepsilon)^{-2.52}\varepsilon^{3}\left(\frac{d_p}{d_c}\right)^{1.5} \tag{19a}$$

The term d_c represents the column diameter.

We note that Eq. 17 is expected to be valid over the same range of L and G values as the underlying experimental correlations. In particular, the correlation of Rao et al. for concurrent downflow has been validated mostly for the air/water system and only down to G = 0.16 kg/m^2.s.

We now write f_{gl}^0 in the following form

$$f_{gl}^0=\beta_0\left(v_g^0-v_l^0\right)=\beta_0 u_{r0} \tag{20}$$

In Eq. 20, the mesoscale phase velocities are assumed equal to the interstitial velocities

$$v_g^0=\frac{V_{sg}}{\varepsilon(1-\varepsilon_l^0)}\quad v_l^0=\frac{V_{sl}}{\varepsilon\varepsilon_l^0} \tag{21}$$

The quantity u_{r0} is defined as the difference between the two interstitial velocities v_g^0 and v_l^0. For a given set of flow conditions (and fluid/bed properties), Eqs. 10 and 11 can be solved for the two unknowns β_0 and ε_l^0. In the linear stability analysis, the value of the first derivative of β_0 with respect to ε_l^0 is needed as well. This value can be found numerically by differentiation of a cubic spline fit to β_0.

Steady-state liquid holdup

Adding Eqs. 10 and 11 and substituting Eqs. 9a and 12 for the liquid–solid interaction force and the total pressure drop, respectively, we get

$$\varepsilon_l^0=\sqrt{A_{ls}/-\left.\frac{dp}{dx}\right]_{f_0}} \tag{22}$$

In Eq. 22, the frictional pressure drop is given by the modified correlation of Motil et al. (Eq. 17). We show later that Eqs. 17 and 22 predict an increase in the liquid holdup with a decrease in gravity level, under similar flow conditions.

Closure relation for H

As discussed previously, we use Eq. 6a in combination with the correlation of Wild et al.[22] for the interfacial area per unit volume in the high-interaction regime. This correlation may be rearranged into the following form

$$a_{int}(\varepsilon_l)=K\ a_S\mathrm{Re}_l^{1.05}\ r(\varepsilon_l)^{0.7} \tag{23}$$

In Eq.23, the dimensionless factor K is given by

$$K=1550(1-\varepsilon)^{1.05}\left(\frac{\rho_g}{\rho_l}\right)^{0.35}\left(\frac{a_s d_h}{1-\varepsilon}\right)^{-3.5}Su_l^{-0.7} \tag{24}$$

The terms a_s (external area of particles and wall per unit reactor volume) and d_h (Krischer and Kast hydraulic diameter) in the righthand side of Eqs. 23 and 24 are defined as follows

$$a_s=\frac{6(1-\varepsilon)}{\varphi d_p}+\frac{4}{d_c};\ d_h=d_p\sqrt[3]{16\varepsilon^3/9\pi(1-\varepsilon)^2} \tag{25}$$

In the aforementioned equation, φ represents the sphericity factor (equal to 1 for spheres), and d_c the column diameter (we use a value of 40 mm for the effective diameter of the column used by Motil[3] to generate the flow transition data). The term $r(\varepsilon_l)$ is the dimensionless ratio of the gas and liquid superficial velocities

$$r(\varepsilon_l)=\frac{V_{sg}}{V_{sl}} \tag{26}$$

For a given set of fluid/bed properties, Motil et al.[2,3] generated their flow-regime transition data by varying the gas flow rate at constant liquid velocity, which suggests that the most natural way to express the ε_l dependence of a_{int} is that given in Eq. 23. We found that the following expression for the prefactor C in Eq. 6a leads to a sufficiently accurate prediction of the bubble to pulse transition for the entire range of fluid properties, flow conditions, and gravity levels covered by the data of Motil et al.

$$C=30\left(1+2Bo^{2/5}\right)\left(We_l\right)^{2/5} \tag{27}$$

The Bond and liquid Weber numbers in Eq. 27 are defined as follows

$$Bo=\frac{\rho_l g d_p^2}{\sigma};\ We_l=\frac{\rho_l V_{sl}^2 d_p}{\sigma(1-\varepsilon)^2} \tag{28}$$

Substitution of Eq. 27 into Eq. 6a leads to the following closure equation for H

$$H=30\left(1+2Bo^{2/5}\right)\left(We_l\right)^{2/5}\frac{a_{int}(\varepsilon_l)}{3\varepsilon(1-\varepsilon_l)} \tag{29}$$

The experimental correlation for the interfacial area per unit volume, which underlies Eq. 29, has been validated only under normal gravity conditions (downflow). However, we are not aware of any similar information for operation under reduced gravity. In any case, the dependence of H on the liquid saturation when G varies at constant L, as provided in Eq. 29, is sufficient for the purposes of the linear stability analysis provided that the magnitude is increased by the factor C. The liquid Weber number factor in C is sufficient to account for variations of the profile with liquid flow, whereas the Bond number factor accounts for the gravity dependence. As for packing size dependence, Eq. 29 may be improved to avoid the slight over prediction of the transition for small packing sizes (see Results and Discussion).

Summary of the 1-D model equations

The continuity equations of the 1-D model may be written as

$$\frac{\partial\varepsilon_l}{\partial t}+v_l\frac{\partial\varepsilon_l}{\partial x}+\varepsilon_l\frac{\partial v_l}{\partial x}=0;\ \text{(Liquid)} \tag{30}$$

$$-\left(\frac{\partial\varepsilon_l}{\partial t}+v_g\frac{\partial\varepsilon_l}{\partial x}\right)+(1-\varepsilon_l)\frac{\partial v_g}{\partial x}=0;\ \text{(Gas)} \tag{31}$$

The momentum equations are given by

$$\rho_l\frac{D_l v_l}{Dt}=-\varepsilon_l\frac{\partial p_l}{\partial x}+\mu_{eff}\frac{\partial\left(\varepsilon_l\frac{\partial v_l}{\partial x}\right)}{\partial x}-\frac{A_{ls}}{\varepsilon_l^2}+\beta(\varepsilon_l)\left(v_g-v_l\right)+\rho_l g=0;\ \text{(Liquid)} \tag{32}$$

$$(1-\varepsilon_l)\left[\rho_g\frac{D_g v_g}{Dt}-\rho_l\frac{D_l v_l}{Dt}\right]=-(1-\varepsilon_l)\frac{\partial p_g}{\partial x}-\beta(\varepsilon_l)\left(v_g-v_l\right)+(1-\varepsilon_l)(\rho_g-\rho_l)g;\quad \text{(Gas)} \tag{33}$$

The derivative terms with capital D refer to material derivatives. Equations 32 and 33 may be combined to eliminate the pressure gradient terms using Eq. 5

$$\rho_l\left(1-\varepsilon_l^2\right)\frac{D_l v_l}{Dt}-\rho_g(1-\varepsilon_l)\varepsilon_l\frac{D_g v_g}{Dt}=2\sigma\varepsilon_l(1-\varepsilon_l)H'(\varepsilon_l)\frac{\partial\varepsilon_l}{\partial x}+\mu_{eff}(1-\varepsilon_l)\frac{\partial\left(\varepsilon_l\frac{\partial v_l}{\partial x}\right)}{\partial x}-A_{ls}\frac{(1-\varepsilon_l)}{\varepsilon_l^2}+\beta(\varepsilon_l)\left(v_g-v_l\right)+\left[\rho_l\left(1-\varepsilon_l^2\right)-\rho_g\varepsilon_l(1-\varepsilon_l)\right]g \quad (34)$$

The aforementioned equations apply to both down flow (g positive, i.e., in the direction of flow), and up flow (g negative, i.e., in the direction opposing the flow). The effective viscosity μ_{eff} can be expected to depend on ε_l, and an appropriate closure equation is required in principle. For simplicity, we use an average value that we estimate in two different ways in order to assess the sensitivity of the model predictions to this parameter. As shown in Tables 3–6, the predicted bubble-to-pulse transition is insensitive to the value of μ_{eff}. However, the wavelength of the fastest growing wave shortly after transition (and, more generally, the growth rate vs. wave number profile such as shown later) is highly sensitive to the value of μ_{eff} in the case of water, although this sensitivity decreases in the case of the more viscous liquids (Table 4). In contrast, the phase velocity of the fastest growing wave seems to be rather insensitive to the choice of μ_{eff} regardless of the value of liquid viscosity. As a result, an extension of this model to the nonlinear regime to determine pulse characteristics will require a more detailed investigation of this parameter. The first estimate of μ_{eff} is based on a scaling argument proposed by Dankworth et al.[15]

$$\mu_{eff}=\rho_l d_p V_{sl} \quad (35a)$$

The second estimate assumes the same viscosity coefficients as those corresponding to the liquid on the continuum scale

$$\mu_{eff}=\lambda_l+\frac{4}{3}\mu_l \quad (35b)$$

For water, we use $\mu_l=0.001$ kg/m.s and $\lambda_l=0.00293$ kg/m.s. For the viscous liquids in Table 4, we use $\lambda_l=0$ (since no information is available).

Linear stability analysis

Assuming small perturbations of the base state in the form of normal modes, linearization of the equations of continuity and momentum conservation (for details of the procedure, see for example Grosser et al.[14]), and choice of a suitable combination of the gas and liquid linearized equations, lead to the following characteristic equation for the growth (or decay) of perturbations

$$As^2-\left(a-A''+ib\right)s+[c+d+i(e-f)]=0 \quad (36)$$

where the coefficients are given by

$$A=\frac{-\rho_l(1+\varepsilon_l^0)}{(\varepsilon_l^0)^2}-\frac{\rho_g}{(1-\varepsilon_l^0)};\quad a=\frac{1}{\varepsilon_l^0}\mu_{eff}k^2 \quad (37)$$

$$A''=-\frac{\beta(\varepsilon_l^0)}{\left[\varepsilon_l^0(1-\varepsilon_l^0)\right]^2} \quad (38)$$

$$b=2\left[\frac{v_l^0\rho_l(1+\varepsilon_l^0)}{(\varepsilon_l^0)^2}+\frac{\rho_g v_g^0}{(1-\varepsilon_l^0)}\right]k;\quad c=\left[\frac{(v_l^0)^2\rho_l(1+\varepsilon_l^0)}{(\varepsilon_l^0)^2}+\frac{\rho_g(v_g^0)^2}{(1-\varepsilon_l^0)}\right]k^2 \quad (39)$$

$$d=2\sigma H'\left(\varepsilon_l^0\right)k^2 \quad (40)$$

$$e=\left\{\frac{1}{\varepsilon_l^0(1-\varepsilon_l^0)}\frac{dp_0}{dx}-\frac{2A_{ls}}{\left(\varepsilon_l^0\right)^4}-\frac{1}{\varepsilon_l^0(1-\varepsilon_l^0)}\left[\beta_0'\left(v_g^0-v_l^0\right)+\beta_0\left(\frac{v_g^0}{1-\varepsilon_l^0}+\frac{v_l^0}{\varepsilon_l^0}\right)\right]+\frac{\left(\rho_l-\rho_g\right)g}{1-\varepsilon_l^0}\right\}k \quad (41)$$

$$f=\frac{v_l^0}{\varepsilon_l^0}\mu_{eff}k^3 \quad (42)$$

The terms β_0, β_0', and $H'\left(\varepsilon_l^0\right)$ are defined as follows

$$\beta_0=\beta\left(\varepsilon_l^0\right);\quad \beta_0'=\frac{d\beta}{d\varepsilon_l}\Big]_{\varepsilon_l^0};\quad H'\left(\varepsilon_l^0\right)=\frac{dH}{d\varepsilon_l}\Big]_{\varepsilon_l^0} \quad (43)$$

In Eqs. 36–42 we assumed solutions of the form

$$\varepsilon_1=\hat{\varepsilon}_1 e^{st+ikx};\quad i=\sqrt{-1} \quad (44)$$

The complex eigenvalues, s, are given by

$$s=\xi-i\eta \quad (45)$$

where ξ is the growth rate of the disturbance and η the angular frequency. The corresponding phase velocity of the disturbance is given by

$$V_p=\frac{\eta}{k}\ . \quad (46)$$

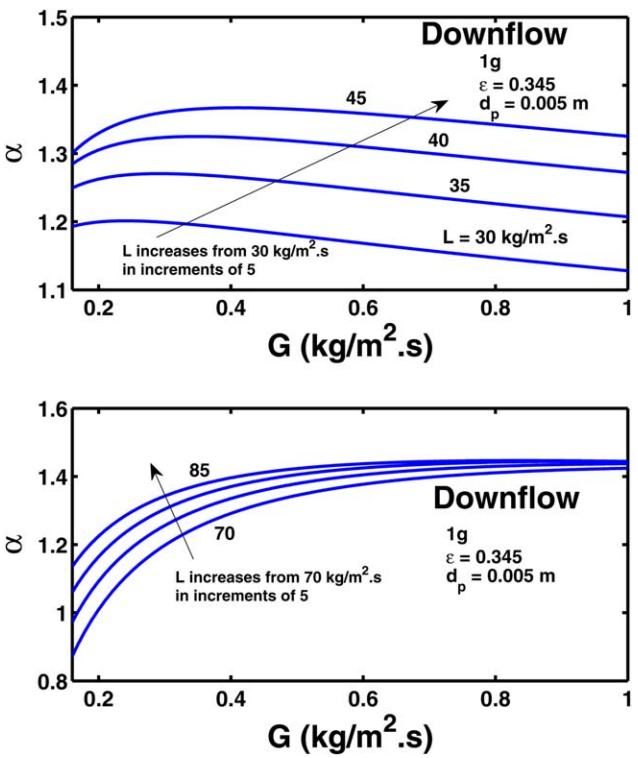

Figure 1. Sample profiles of the parameter α in the downflow configuration under normal gravity conditions (air/water system).

[Color figure can be viewed in the online issue, which is available at wileyonlinelibrary.com.]

Table 1. Maximum in α and Location of the Bubble-to-Pulse Transition in Concurrent Downflow under Normal Gravity Conditions (Air/Water System)

L (kg/m^2.s)	G_{Motil} (kg/m^2.s)	$G_{\alpha max}$ (kg/m^2.s)	α_{max}
$d_p = 0.005$ m (Bo = 3.36)			
30	0.24	0.25	1.20
35	0.29	0.30	1.27
40	0.35	0.34	1.33
45	0.41	0.38	1.37
50	0.48	0.42	1.40
$d_p = 0.002$ m (Bo = 0.54)			
15	0.09	0.10	0.81
25	0.12	0.16	1.00
30	0.13	0.19	1.05
38	0.17	0.25	1.10

Results and Discussion

Steady-state predictions

Pressure Drop and Liquid Holdup. The frictional pressure drop correlation given in Eq. 17 summarizes both reduced and normal gravity experimental observations in a single expression through the use of the parameter α in the "dynamic interaction term". As mentioned previously, under microgravity conditions, this parameter takes a constant value of 0.8, while in normal gravity it varies with both system properties and flow conditions. Figure 1 shows the typical variation of α with G for increasing values of L in the downflow configuration under normal gravity. This parameter generally goes through a maximum whose location shifts to higher values of G as L increases. The maximum seems to disappear at very high values of L ($L > 70$ kg/m^2.s). Table 1 shows a close agreement between the location of this maximum and the bubble to pulse transition data of Motil et al.[2,3] for the air/water system (normal gravity downflow, $d_p = 5$ mm or $Bo = 3.36$). When the packing size is decreased to 2 mm ($Bo = 0.54$), the location of the maximum in α is still within 50%, or less, of the bubble-pulse transition as defined by Motil et al. The greater deviation for the smaller packing size is to be expected since the maximum in α disappears completely (becomes "very diffuse") as the Bond number tends to zero, and can no longer be used to gauge the transition. For the same reason, the disappearance of the maximum at high values of L does not necessarily imply the disappearance of the bubble-to-pulse transition. More work

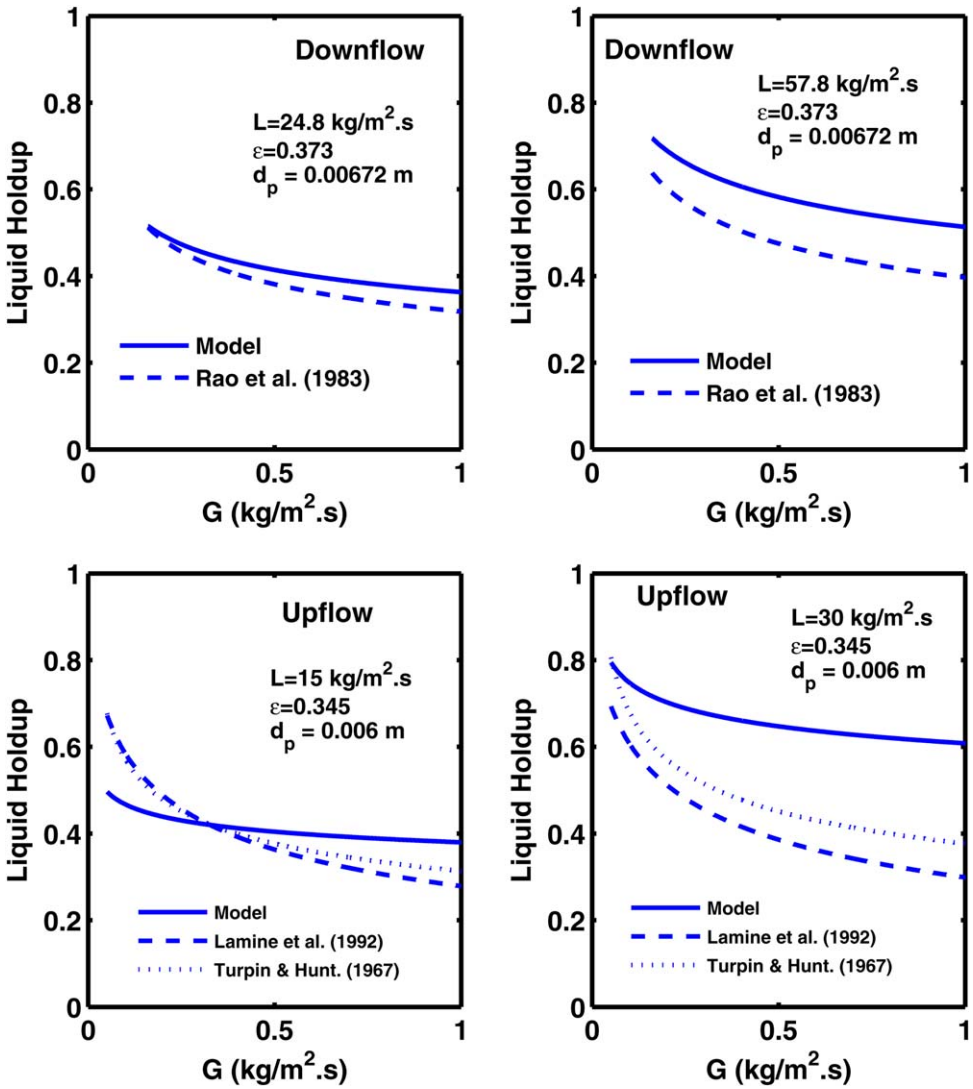

Figure 2. Comparison of model predictions for liquid holdup with experimental correlations for both downflow and upflow in normal gravity (air/water system).

[Color figure can be viewed in the online issue, which is available at wileyonlinelibrary.com.]

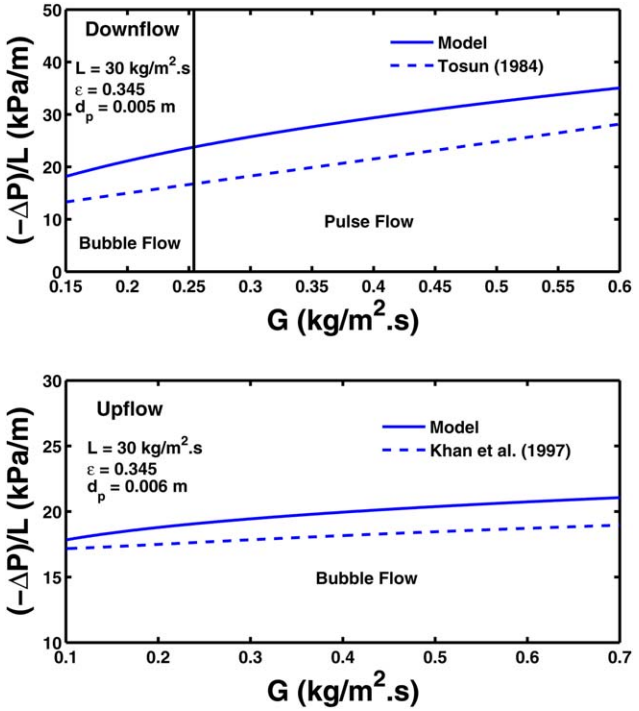

Figure 3. Comparison of model predictions for the total pressure drop with Tosun's[28] (downflow) and Khan et al.[25] (upflow) correlations (air/water system).

[Color figure can be viewed in the online issue, which is available at wileyonlinelibrary.com.]

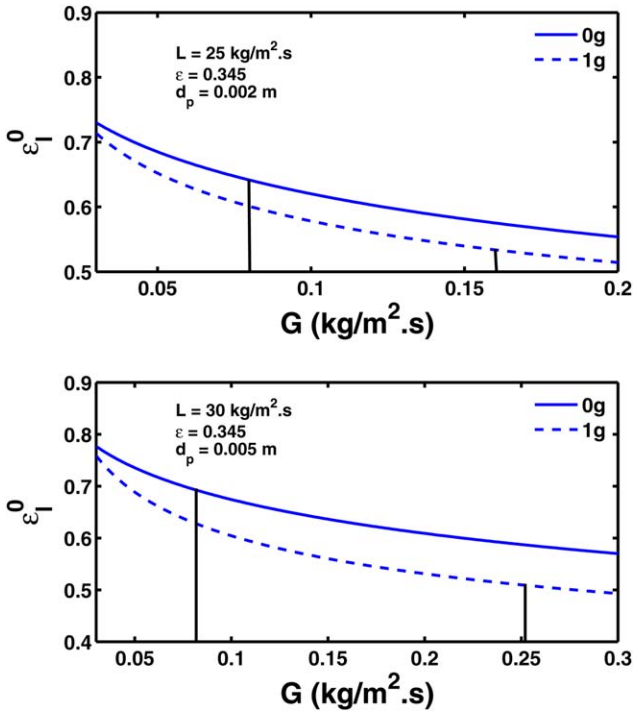

Figure 4. Impact of gravity on liquid holdup (air/water, $d_p = 2$ mm and 5 mm).

The vertical lines represent the experimentally observed bubble to pulse transition. [Color figure can be viewed in the online issue, which is available at wileyonlinelibrary.com.]

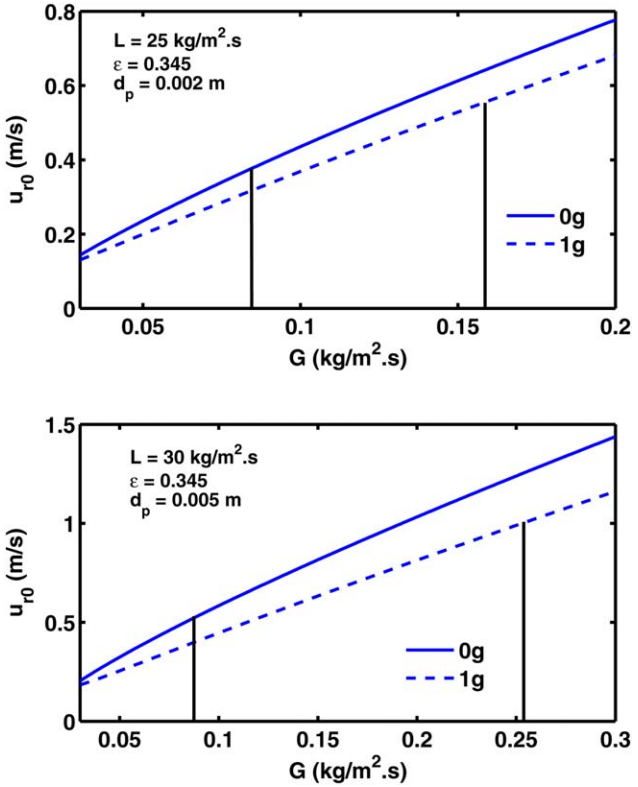

Figure 5. Difference in interstitial velocities ($u_{r0} = v_g^0 - v_l^0$) between the gas and liquid phases (air/water, $d_p = 2$ mm and 5 mm).

The vertical lines represent the experimentally observed bubble to pulse transition. [Color figure can be viewed in the online issue, which is available at wileyonlinelibrary.com.]

is needed to determine the range of L values over which there may be a close correlation between the location of the maximum in α and the bubble-to-pulse transition in concurrent downflow under normal gravity conditions. In the case of upflow (not shown), the maximum becomes visible only at very high values of L. The α profiles indicate that the aforementioned transition criterion may be useful only at very large values of L. However, our main focus here is on the downflow configuration and the interpretation of the data obtained by Motil et al. to compare the bubble-pulse transition in microgravity to that in normal gravity with both fluids flowing downward.

In Figure 2, we compare the model predictions for liquid holdup in normal gravity with available correlations for downflow (Rao et al.[6]) and upflow (Lamine et al.[26] and Turpin and Huntington[27]). For downflow, the model is in rather good quantitative agreement with the data of Rao et al.[6] However, in the upflow configuration, the predictions are not in quantitative agreement with the experimental correlations and present a much flatter profile than the latter. In Figure 3, we compare the model predictions for the total pressure drop with Tosun's[28] (downflow) and Khan et al.[25] (upflow) correlations. In the downflow configuration, the model predictions are in quantitative agreement with Tosun's correlation, which was found to describe the normal gravity data of Motil et al. satisfactorily. In the upflow configuration, the apparent agreement of the model with the experimental correlation despite the rather poor predictions for the liquid

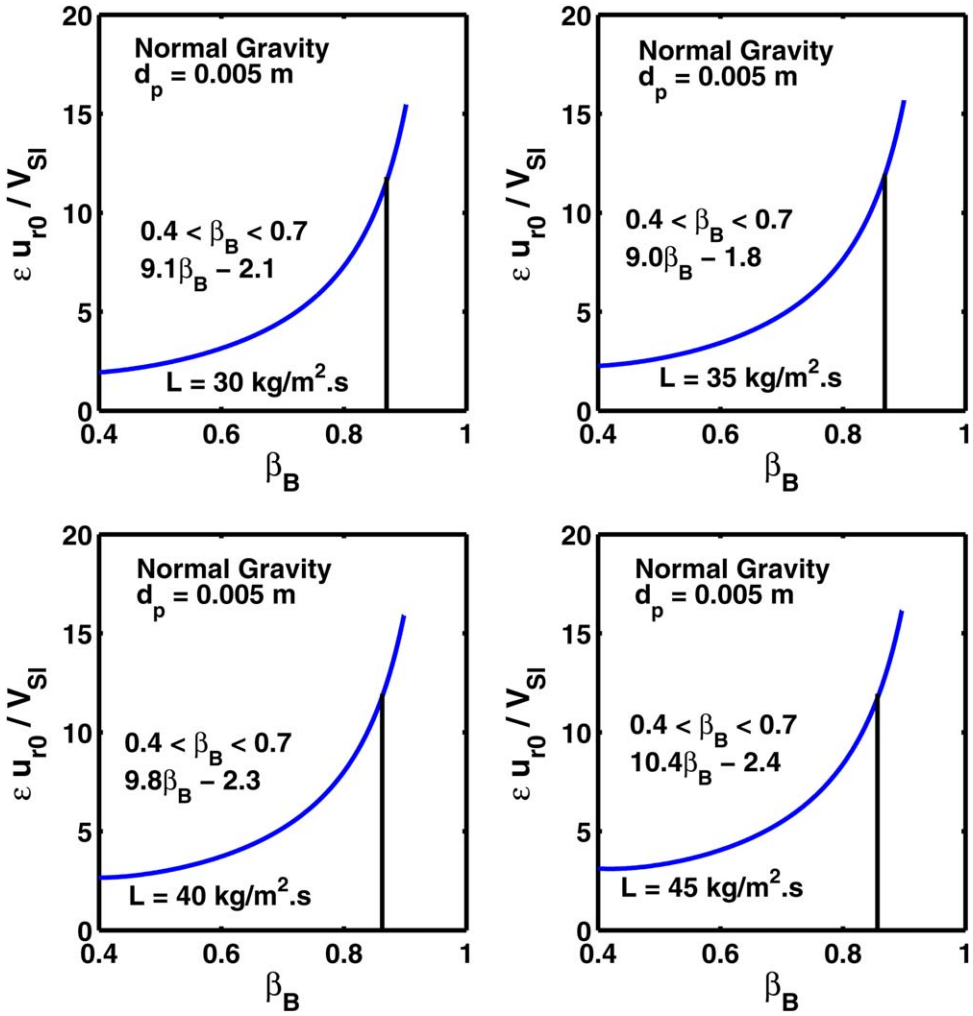

Figure 6. Profiles of $\frac{\varepsilon u_{r0}}{V_{SI}}$ vs. $\beta_B\left(=\frac{r}{r+1}\right)$ under normal gravity conditions (air/water, $d_p = 5$ mm).

The vertical lines represent the experimentally observed bubble to pulse transition. [Color figure can be viewed in the online issue, which is available at wileyonlinelibrary.com.]

holdup suggest that under such flow rates the frictional pressure drop dominates the static head contribution. In the remainder of this article, we focus exclusively on the effect of gravity on bubbly flow and the bubble-to-pulse transition in the downflow configuration, as studied experimentally by Motil.[2,3]

We are not aware of any liquid holdup data under reduced gravity to compare with model predictions. However, for the range of L values used in the experiments of Motil et al. ($L < 50$ kg/m^2.s), the frictional pressure drop in the downflow configuration is seen to increase with gravity level ($\alpha > 0.8$) for the same flow conditions. We then expect (see Eq. 22) the liquid holdup to increase as gravity is decreased from normal levels while keeping the same flow conditions. Figure 4 illustrates the predicted decrease of liquid holdup with gravity level. This decrease is predicted to become more significant as the size of the packing increases. The two vertical lines in these and subsequent figures indicate the location of the experimentally observed bubble-to-pulse transition at the two gravity levels.[2,3] In downward flow, we would expect the buoyancy force due to gravity to slow down the gas phase relative to the liquid phase, which would result in a smaller relative velocity of the phases and a larger gas fraction, hence, a lower liquid holdup. We note that the predicted liquid holdup trends are consistent with the observations of Larachi and Munteanu,[29] who measured higher liquid holdup values as they decreased the gravity level artificially by applying magnetic forces to the flow. Bordas et al.[23] conjectured that the difference between the gas and liquid interstitial velocities as defined by Eq. 21 may be an appropriate measure of the relative velocities of the phases at mesoscale, even at high-gas volume fractions such as those of relevance in this work. In Figure 5, we plot this velocity difference as a function of G for a fixed value of L. As shown in the figure, this velocity difference increases as the gravity level decreases, which supports the idea that it may be an appropriate measure for the relative velocity of the phases at mesoscale. We also note from Figures 4 and 5 that the model produces a consistent picture (higher liquid holdup and relative velocity under microgravity) down to a G value of about 0.03 kg/m^2.s to 0.06 kg/m^2.s, even though the underlying normal gravity correlation (Rao et al.[6]) has been validated only down to $G = 0.16$ kg/m^2.s. In Figure 6, we show profiles of the normalized velocity $\frac{\varepsilon u_{r0}}{V_{sl}}$ vs. the parameter $\beta_B = \frac{r}{1+r}$ for one of the air/water systems studied by Motil et al.[2,3] Under normal gravity conditions, all the curves show an almost identical profile, regardless of the liquid

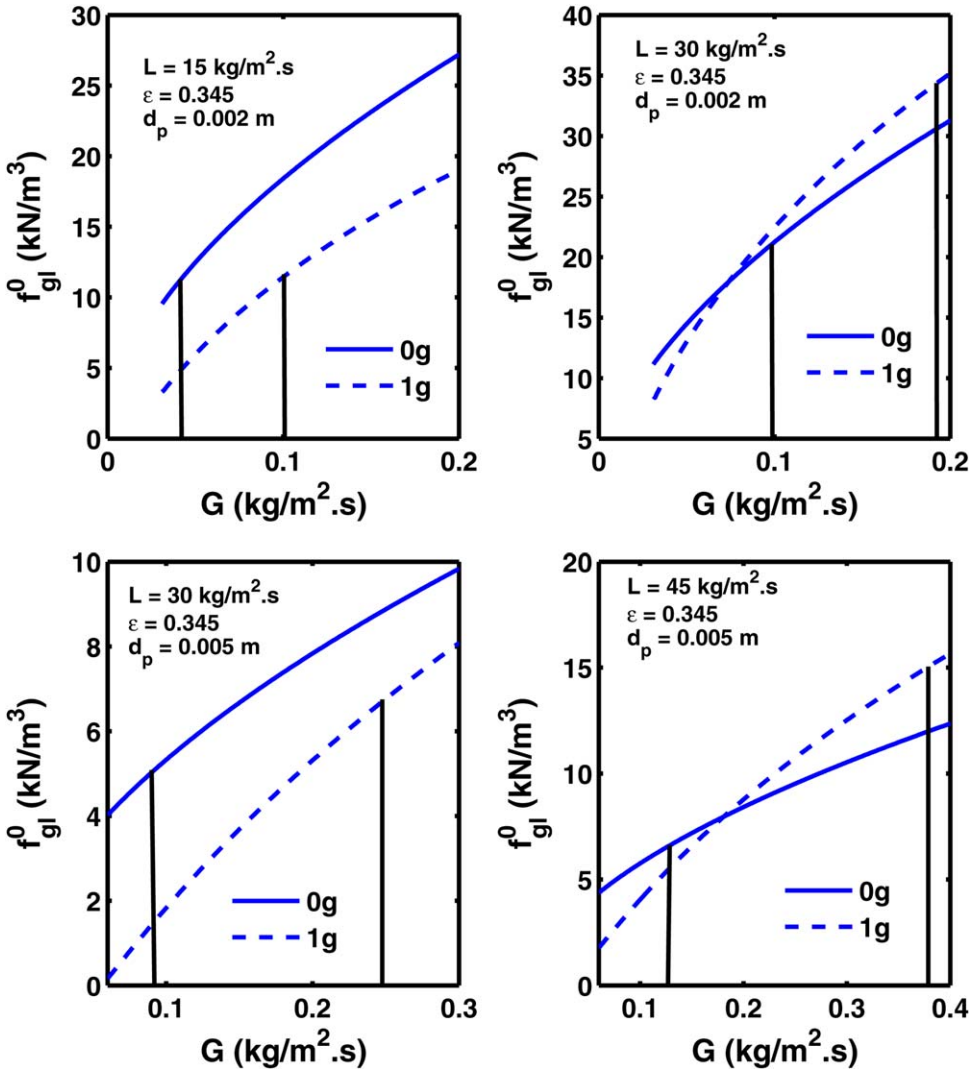

Figure 7. Impact of gravity on the gas-liquid interaction force density (air/water, $d_p = 2$ mm and 5 mm).

The vertical lines represent the experimentally observed bubble to pulse transition. [Color figure can be viewed in the online issue, which is available at wileyonlinelibrary.com.]

superficial velocity. This is consistent with the experimental observations reported by Bordas et al.[23] Moreover, for $\beta_B > 0.4$, the model generated curves are in reasonable quantitative agreement with the experimental curve presented by these authors. In particular, the linear fits in the region $0.4 < \beta_B < 0.7$ compare favorably with the coefficients reported by Bordas et al.[23] for a slightly larger interval, namely, 6.7 for the slope and -1.9 for the intercept.

Liquid-gas and liquid–solid Interaction Force Densities. In this section, we examine in more detail, the conditions under which the model (uniform) steady-state solution is consistent with a concurrent bubbly flow. If the difference in interstitial velocities (Eq. 21) is representative of the relative velocity of the phases at mesoscale and the flow is bubbly (i.e., the buoyancy forces are accounted for in the momentum balance), a consistent solution should yield the same sign for the relative velocity u_{r0} and the term f_{gl}^0 in Eqs. 10 and 11. This term represents the average force (per unit volume) exerted by the gas on the liquid and should be positive (in the flow direction) when the gas is flowing faster, and negative when the gas is flowing slower. At very low-gas flow rates, and for a given liquid superficial velocity, we should then expect f_{gl}^0 to switch from a negative value to a positive value at about the same gas-flow rate where the difference in intersiticial velocities switches signs.

Under reduced gravity conditions (± 0.02 g with average $Bo = 0$), f_{gl}^0 is always predicted to be positive even in the small low G interval where the difference in interstitial velocities is predicted to be negative. A possible explanation is that this velocity difference may no longer be representative of the relative velocity at mesoscale at very low-gas flow rates (G less than about 0.015 kg/m^2.s). However, this does not affect the validity of the model for providing a base state for predicting the bubble-to-pulse transition from linear stability considerations. Indeed, for L greater or equal to 5 kg/m^2.s, the bubble to pulse transition is observed at a value of G that is greater than the threshold value beyond which both f_{gl}^0 and the difference in interstitial velocities are positive. Under normal gravity conditions, the model will provide a valid description of the base state (both u_{r0} and f_{gl}^0 are positive) for values of $G > 0.03$ kg/m^2.s–0.06 kg/m^2.s. A more stringent self-consistency criterion, based on the profile of the parameter β_0 defined in Eq. 20, is given in the next section.

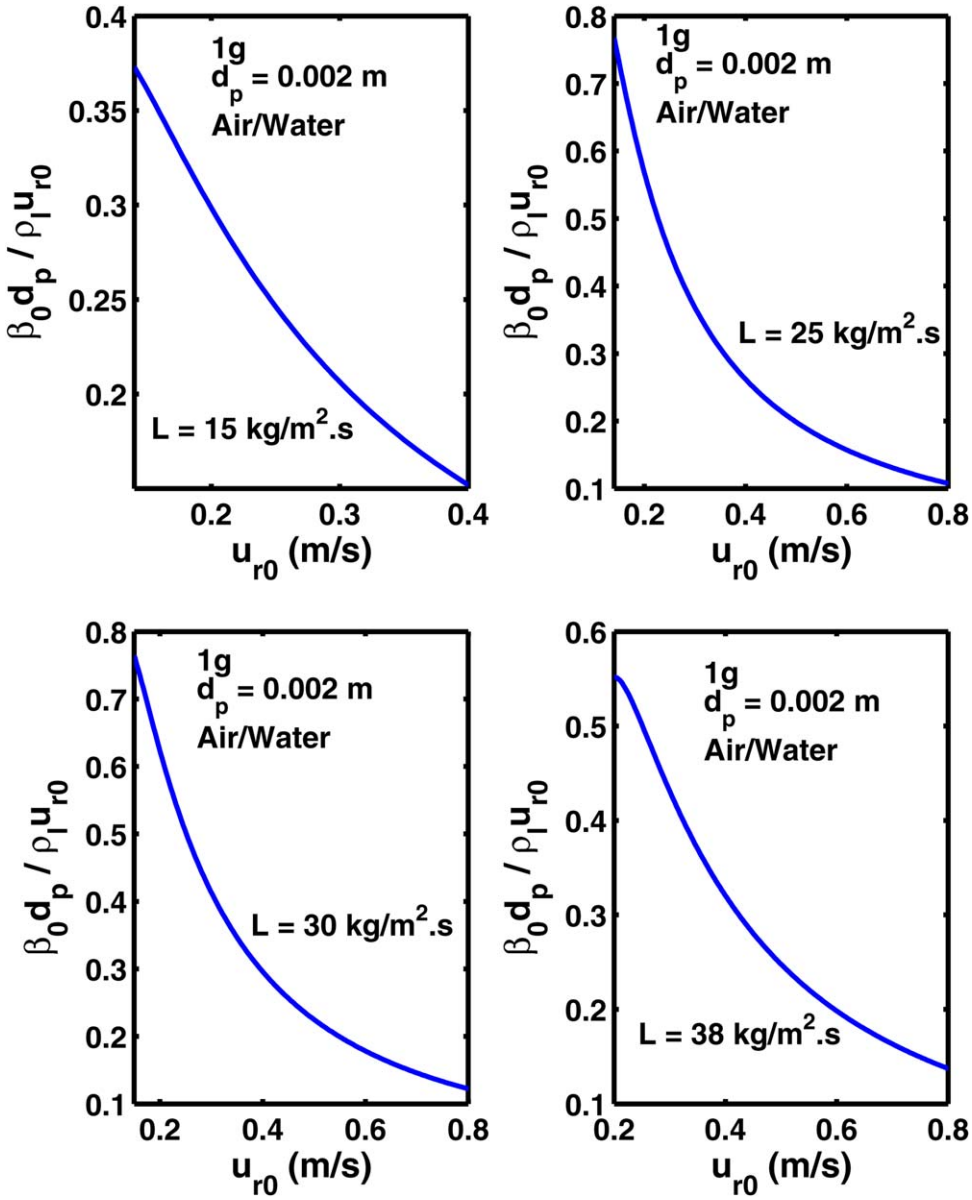

Figure 8. Profiles of $\frac{\beta_0 d_p}{\rho_l u_{r0}}$ vs. $u_{r0}=v_g^0-v_l^0$ for the air/water system under normal gravity conditions ($d_p=2$ mm).

[Color figure can be viewed in the online issue, which is available at wileyonlinelibrary.com.]

Last, the predicted effect of gravity on the magnitude of the liquid-gas interaction force density (f_{gl}^0) is illustrated in Figure 7. First, we note that for a given liquid flow rate, the gas-liquid interaction increases with G. Also, the profile of f_{gl}^0 is almost independent of L (changes only by a few percent between the low-end and high-end values of L) in zero gravity. In contrast, under normal gravity conditions, this profile changes more noticeably with L (by about a factor of two between the low and high L). The figure also shows that under bubbly conditions, f_{gl}^0 has a higher magnitude in zero gravity at the lower liquid flow rates. At higher values of L, f_{gl}^0 has about the same magnitude at both gravity levels under bubbly flow conditions.

Predicted behavior of β_0 and H. The parameter β_0 is not a dimensionless "drag" coefficient but is introduced in Eq. 20 to show explicitly the dependence of f_{gl}^0 on the relative velocity of the phases at mesoscale. However, this parameter can be used to determine a more conservative lower limit on G for the consistency of model predictions with a concurrent bubbly flow where the gas phase is traveling faster than the liquid phase. For a given system and liquid flow, the lowest G value must be such that both the relative velocity and f_{gl}^0 are positive. To estimate this value, we propose the following approach. In Figure 8, we show a sample plot of the dimensionless quantity $\frac{\beta_0 d_p}{\rho_l u_{r0}}$ vs. $u_{r0}=v_g^0-v_l^0$. As seen in this figure, beyond a given value of the relative velocity (or G), this curve always follows a monotonous profile with an initial rapid decrease as a negative power of the relative velocity followed by a region of slower decrease. For G values in this range, the uniform steady-state solution of the model is consistent with the picture of concurrent bubbly flow where the gas velocity at mesoscale is larger than that of the liquid. For the three air/water systems studied by Motil et al.[2,3] the lower cutoff value for G does not exceed 31% of the observed bubble-to-pulse transition value for $L>7$ kg/m^2.s under microgravity conditions, while for normal gravity it is

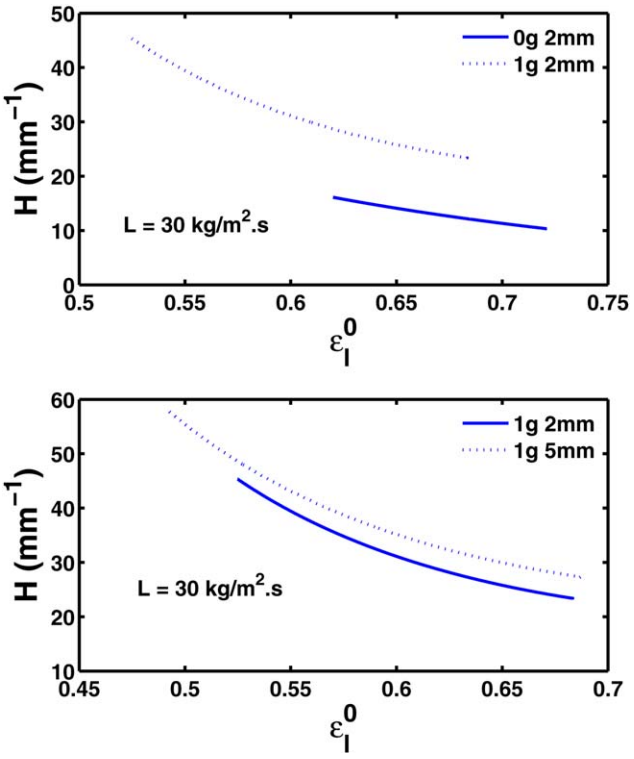

Figure 9. Profiles of the average mean interfacial curvature H under reduced and normal gravity conditions (air/water, $d_p = 2$ mm and 5 mm).

[Color figure can be viewed in the online issue, which is available at wileyonlinelibrary.com.]

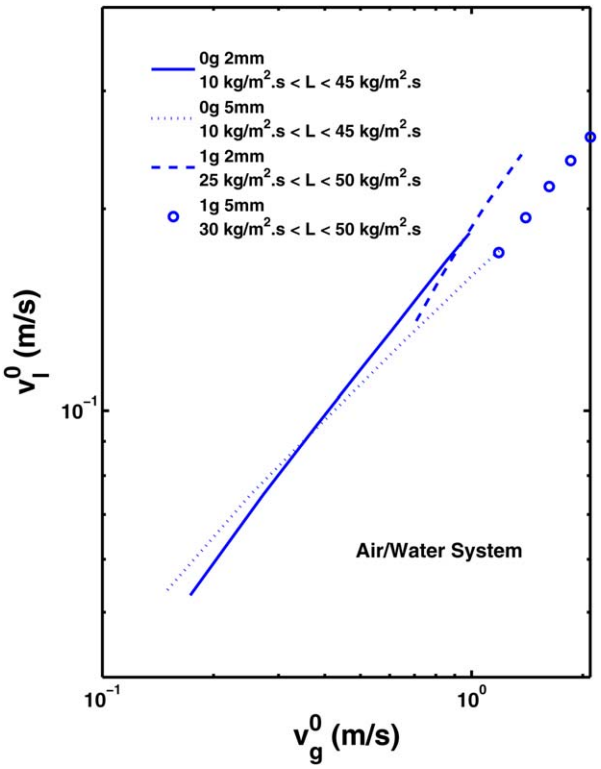

Figure 11. Liquid interstitial velocity versus gas interstitial velocity at the experimentally observed bubble-to-pulse transition (air/water system).

[Color figure can be viewed in the online issue, which is available at wileyonlinelibrary.com.]

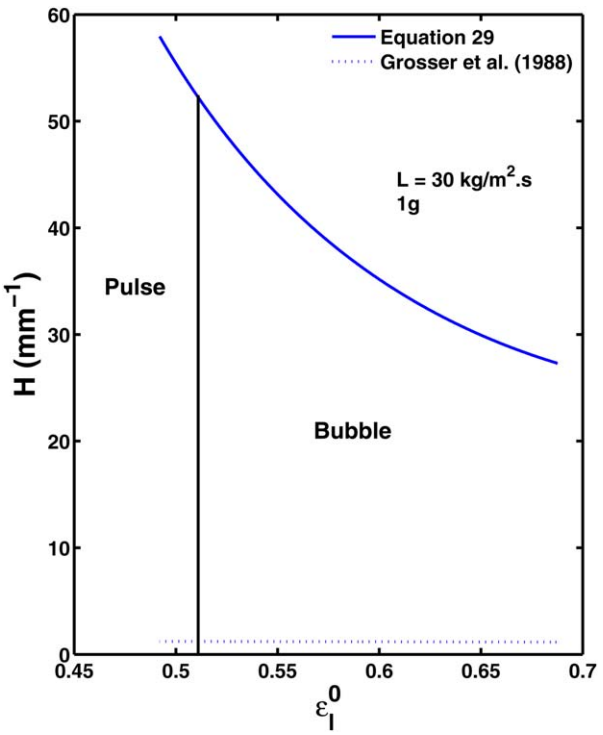

Figure 10. Comparison of H predictions with Grosser et al.[14] under normal gravity conditions (air/water, $d_p = 5$ mm).

Similar trends are observed in reduced gravity. [Color figure can be viewed in the online issue, which is available at wileyonlinelibrary.com.]

less than 30% of that value for a packing size of 2 mm (for $L > 15$ kg/m^2.s), and less than 47% of the transition value for a packing size of 5 mm (for $L > 30$ kg/m^2.s).

Sample profiles for the average curvature H are shown in Figure 9. Inspection of the profiles shows that (1) the predicted value for the capillary pressure under the same flow conditions and for the same packing size increases with gravity level, and (2) the predicted capillary pressure is rather insensitive to packing size for the same flow conditions and gravity level (the values predicted for the two packing sizes, 2 mm and 5 mm, are within about 20% of each other). In Figure 10, we compare the predictions of Eq. 29 with the correlation used by Grosser et al.[14], which is based on the J function (drainage curve) along with an estimate of the bed permeability that is consistent with their closures for the terms f_{gl} and f_{ls}. The figure shows that the magnitude of the slope of H predicted by this closure is much smaller than the value predicted by Eq. 29. A larger variation in the case of the bubble-to-pulse transition is to be expected as the bubbles take on (on average) a more elongated and thin profile with increasing gas flow rate. When the pulse flow is approached from the trickle flow regime, it is reasonable to expect the average curvature to stay roughly of the same order as the inverse of the packing diameter. Therefore, while providing a convenient explicit relationship in terms of the liquid holdup, the closure of Grosser et al.[14] does not show a sufficient rate of increase in the capillary pressure over the relevant range of liquid holdup and, hence, will not predict the observed bubble-to-pulse transitions.

Table 2. Predicted Values of the Ratio of Interstitial Velocities at the Experimentally Observed Bubble-Pulse Transition (Air/Water System)

L (kg/m^2.s)	$\frac{v_g^0}{v_l^0}$ 0g – 2mm	$\frac{v_g^0}{v_l^0}$ 0g – 5mm	$\frac{v_g^0}{v_l^0}$ 1g – 2mm	$\frac{v_g^0}{v_l^0}$ 1g – 5mm	$\rho_g^{avg}\frac{v_g^0}{v_l^0}$ 1g – 2mm	$\rho_g^{avg}\frac{v_g^0}{v_l^0}$ 1g – 5mm
10	3.26	2.77				
15	3.64	3.36				
20	4.00	3.99	5.23			
25	4.32	4.6	5.21			
30	4.62	5.17	5.23	6.89	7.85	8.75
35	4.87	5.76	5.30	7.22	8.27	9.39
40	5.11	6.31	5.39	7.52	8.79	9.93
45	5.36	6.90	5.53	7.86	9.35	10.61
50	5.58	7.42	5.66	8.18	9.91	11.21

Also, the figure shows that the magnitude of H itself, as predicted by Eq. 29, is an order of magnitude larger. We would in fact expect a higher average curvature for the interface in the case of a transition from bubble to pulse since here the curvature is governed mostly by the shape of the constantly distorted and increasingly elongated bubbles in the flow channels.

Impact of gravity and packing size on the bubble-to-pulse transition. The picture of large bubble flow (or "slug" flow) in the pore space, which is based on the observations of Bordas et al.[23] who measured average bubble sizes of the order of the pore space δ even at very low-gas flow rates, is (qualitatively) consistent with the flow regime transition map obtained by Triplett et al.[30] for gas-liquid flow in capillaries. At the lowest gas velocities, these authors observed slug flow for liquid velocities smaller than about 1 m/s and bubbly flow at higher liquid velocities. Using the interstitial velocities as representative of the superficial velocities at the pore level, and considering that the liquid interstitial velocity is typically less than about 0.2–0.3 m/s when the bed is in the "bubbly flow regime", we would then expect "slug flow" at the pore level. As the gas velocity is increased at constant liquid flow, Triplett et al.[30] observed a transition to a "slug-annular" flow when the liquid velocity is less than about 0.3–0.6 m/s (depending on the capillary diameter). As this regime is approached, the bubble size increases leading to coalescence and the development of "wavy-annular" flow. At higher liquid velocities, the flow is seen to transition instead to a "churn" flow, which includes the aerated slug flow pattern. Recent high-speed video taken by Motil et al. (to be published) in the pulse flow regime clearly shows that the liquid-rich pulses are highly aerated with very small bubbles. The gas-rich regions between pulses are harder to visualize, but the videos do not show any strong presence of (small) bubbles. Although, strictly speaking, the map of Triplett et al.[30] applies to capillary channels of non-varying cross section and well-defined geometry, it gives a qualitative picture of what might be happening at the pore level as the bed transitions form bubbly to pulse flow. The flow separates into regions of low-liquid velocity (the so-called gas-rich regions between pulses) where both phases are continuous and regions of high-liquid velocities (the liquid-rich pulses) where the bubbles are very small even at the pore level (almost "froth-like"). In Figure 11, we plot the liquid interstitial velocity versus the gas interstitial velocity at the

Table 3. Bubble-Pulse Transition for Air/Water System ($\pm$0.02g, average $Bo = 0$) and Velocity of Fastest Growing Wave Shortly after the Predicted Transition

L (kg/m^2.s)	G_{Motil} (kg/m^2.s)	ρ_g (kg/m^3)	$\frac{G_{Predicted}}{G_{Motil}}$	ε_l^0 at predicted transition	V_p (m/s)
d_p=5 mm, Su_l=365,000					
10	0.03	1.21	1.02	0.53	0.40
15	0.04	1.21	0.98	0.59	0.62
20	0.06	1.22	0.95	0.63	0.86
25	0.07	1.23	0.92	0.67	1.13
30	0.09	1.24	0.90	0.70	1.41
40	0.12	1.27	0.87	0.74	2.05
50	0.15	1.30	0.85	0.78	2.77
d_p=2 mm, Su_l=146,000					
10	0.03	1.27	1.23	0.53	0.52
15	0.05	1.30	1.23	0.56	0.78
20	0.07	1.34	1.24	0.59	1.07
25	0.08	1.39	1.25	0.62	1.36
30	0.10	1.43	1.27	0.64	1.66
40	0.13	1.52	1.33	0.67	2.31
50	0.17	1.63	1.39	0.69	2.99

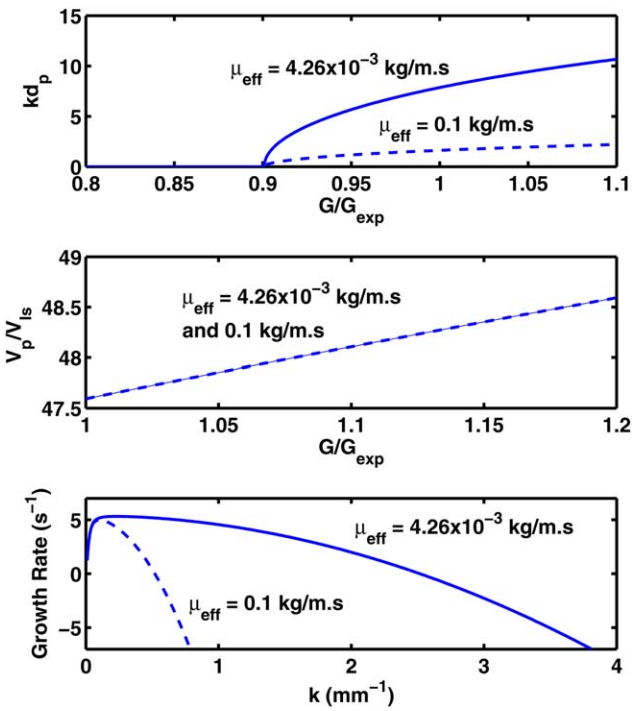

Figure 12. Neutral stability curve (Top) Normalized neutral pulse velocity curve (Middle) Growth rate vs. wave number profile (Bottom).

Air/water system under reduced gravity conditions ($L = 30$ kg/m^2.s, $Bo = 0$). [Color figure can be viewed in the online issue, which is available at wileyonlinelibrary.com.]

Table 4. Bubble-Pulse Transition for Air/Viscous Liquid Systems (±0.02g, average $Bo = 0$) and Velocity of Fastest Growing Wave Shortly after the Predicted Transition

L (kg/m^2.s)	G_{Motil} (kg/m^2.s)	ρ_g (kg/m^3)	$\frac{G_{Predicted}}{G_{Motil}}$	ε_l^0 at predicted transition	V_p (m/s)
d_p=5 mm, μ_l=0.02 kg/m.s, ρ_l=1192 kg/m^3, σ=0.062 kg/s^2 Su_l=900					
10	0.07	1.27	0.69	0.75	1.04
15	0.11	1.31	0.68	0.77	1.56
20	0.14	1.35	0.68	0.78	2.09
30	0.22	1.43	0.70	0.79	3.16
40	0.29	1.51	0.72	0.80	4.26
d_p=2 mm, μ_l=0.0096 kg/m.s, ρ_l=1158 kg/m^3, σ=0.067 kg/s^2 Su_l=1680					
10	0.07	1.47	1.08	0.71	1.07
15	0.10	1.61	1.15	0.72	1.59
20	0.13	1.75	1.24	0.72	2.09
30	0.20	2.05	1.44	0.73	3.08
d_p=5 mm, μ_l=0.0096 kg/m.s, ρ_l=1158 kg/m^3, σ=0.067 kg/s^2 Su_l=4200					
10	0.06	1.24	0.74	0.68	0.74
15	0.09	1.27	0.73	0.70	1.12
20	0.11	1.29	0.72	0.72	1.50
30	0.17	1.34	0.71	0.74	2.30
40	0.23	1.39	0.72	0.76	3.14
d_p=5 mm, μ_l=0.0041 kg/m.s, ρ_l=1104 kg/m^3, σ=0.07 kg/s^2 Su_l=23000					
10	0.04	1.22	0.82	0.61	0.55
15	0.07	1.24	0.80	0.64	0.83
20	0.09	1.25	0.78	0.66	1.13
30	0.13	1.28	0.76	0.70	1.77
40	0.18	1.32	0.76	0.73	2.46

observed bubble-to-pulse transition. This representation is analogous to the flow regime map of Triplett et al.[30] in which the interstitial velocities play the role of the superficial velocities in the capillary. Inspection of Figure 11 and Table 2 clearly shows the following (1) under microgravity, the ratio of the gas to liquid interstitial velocities at the observed transition is about the same for both packing sizes (this is especially true for L values less than about 40 kg/m^2.s, which is the range that plays a dominant role in Motil's microgravity transition correlation), (2) under normal gravity, the ratio of the gas to liquid interstitial velocities is smaller for the smaller packing size (by a factor that is roughly equal to the ratio of the average gas densities in the bed, as shown in Table 2), and (3) for a given packing size, the ratio of the gas to liquid interstitial velocities is about the same under microgravity and normal gravity.

One of the main observations made by Motil et al.[2,3] is that, for the same packing size, the transition to pulse flow occurs at a higher value of G/L in normal gravity. Based on observation (3) earlier, we write

Table 5. Bubble-Pulse Transition for Air/Water System (1g, $d_p = 2$ mm, $Bo = 0.54$) and Velocity of Fastest Growing Wave Shortly after the Predicted Transition

L (kg/m^2.s)	G_{Motil} (kg/m^2.s)	ρ_g (kg/m^3)	$\frac{G_{Predicted}}{G_{Motil}}$	ε_l^0 at predicted transition	V_p (m/s)
15	0.10	1.32	1.19	0.50	1.36
20	0.13	1.38	1.22	0.51	1.81
30	0.19	1.53	1.31	0.52	2.77
35	0.23	1.60	1.37	0.53	3.28
40	0.26	1.68	1.44	0.54	3.82
50	0.32	1.84	1.59	0.56	4.95

Table 6. Bubble-Pulse Transition for Air/Water System (1g, $d_p = 5$ mm, $= 3.36$) and Velocity of Fastest Growing Wave Shortly after the Predicted Transition

L (kg/m^2.s)	G_{Motil} (kg/m^2.s)	ρ_g (kg/m^3)	$\frac{G_{Predicted}}{G_{Motil}}$	ε_l^0 at predicted transition	V_p (m/s)
30	0.25	1.27	0.90	0.52	2.73
35	0.30	1.29	0.91	0.53	3.20
40	0.34	1.32	0.92	0.55	3.68
45	0.38	1.34	0.94	0.56	4.18
50	0.42	1.37	0.96	0.57	4.69

$$\left(\frac{v_g^0}{v_l^0}\right)_{0g} \approx \left(\frac{v_g^0}{v_l^0}\right)_{1g} \tag{47}$$

Noting that, for a given packing size, the average gas density in the bed is rather insensitive to gravity level, Eq. 47 leads to

$$\left(\frac{G}{L}\right)_{0g}\left(\frac{\varepsilon_l^0}{1-\varepsilon_l^0}\right)_{0g} \approx \left(\frac{G}{L}\right)_{1g}\left(\frac{\varepsilon_l^0}{1-\varepsilon_l^0}\right)_{1g} \tag{48}$$

Since, for the same flow conditions, the model predicts a higher liquid holdup under microgravity conditions, Eq. 48 leads to the observed result

$$\left(\frac{G}{L}\right)_{0g} < \left(\frac{G}{L}\right)_{1g} \tag{49}$$

As a numerical example, for $L = 30$ kg/m^2.s and a packing size of 5 mm, Eq. 48 predicts a G/L ratio that is about 2.1 times higher under normal gravity, which compares favorably with the observed factor of 2.8 (see Tables 3 and 5). Similarly, it can be shown that features (1) and (2) are

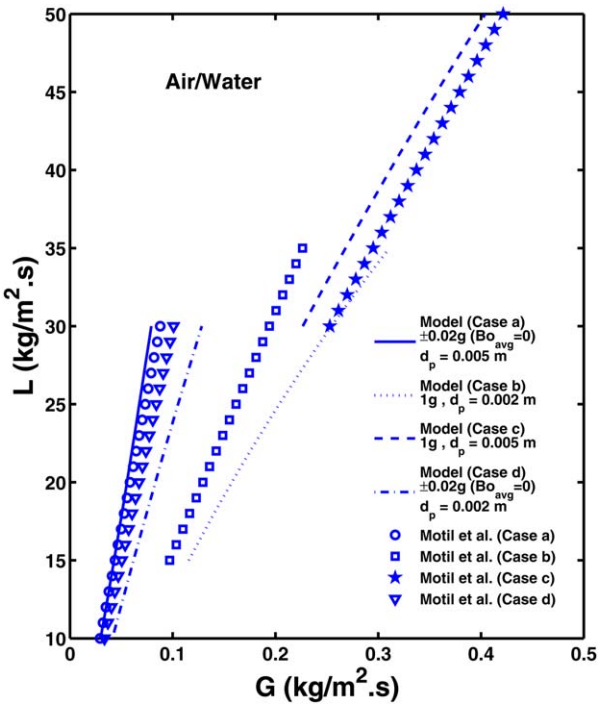

Figure 13. Comparison of model predictions for the bubble-to-pulse transition with the empirical correlations of Motil et al.[2] and Motil[3].

[Color figure can be viewed in the online issue, which is available at wileyonlinelibrary.com.]

consistent with the observations of Motil et al. regarding the effect of packing size on the bubble-to-pulse transition.

Since, for a given packing size, the ratio of the gas to liquid interstitial velocities at the observed transition is rather independent of the gravity level, the impact of gravity on the transition lies in the extent to which it dictates the average value of liquid holdup in the bed. For a given liquid flow and packing size, the presence of gravity requires a higher value of gas flow to reach the threshold ratio of the interstitial velocities which is needed for the transition.

Linear stability predictions

Table 3 shows the model predictions for the bubble-pulse transition for an air–water system under microgravity conditions (± 0.02 g with average $Bo = 0$) and compares these values with the experimental correlation of Motil et al.[2,3] The agreement is seen to be satisfactory for values of L larger than 10 kg/m^2.s. Also shown in Table 3 is the velocity of the fastest growing wave shortly after the predicted transition. For $L = 15$ kg/m^2.s, the model predicts a wave velocity of 0.62 m/s, which compares favorably with measured pulse velocities at similar flow rates (Motil et al., to be published). In Figure 12, we show typical results for the neutral stability curve, the neutral pulse velocity, and the growth rate vs. wave number curve for a point beyond the transition. Similar results are shown in Table 4 for various air/viscous liquid systems under microgravity conditions (average $Bo = 0$). The liquid viscosity in these systems varies from about 4 to 20 times the viscosity of water. The model again predicts the transition with reasonable accuracy. The values predicted for the phase velocity of the fastest growing wave are larger than those predicted for water at similar liquid flow rates. However, it should be noted that the values of the gas flow rates are larger in the case of the viscous liquids.

Tables 5 and 6 show results for the air/water system under normal gravity conditions for two packing sizes ($d_p = 2$ mm in Table 5, $d_p = 5$ mm in Table 6). The model predictions agree well with the experimental correlations. A comparison of Tables 3 and 6 shows that velocity of the fastest growing wave increases with gravity level for the same flow/bed conditions, probably because of the higher gas flow rates that are required for the transition at normal gravity. Figure 13 compares the model predictions for the bubble-pulse transition (air/water) with the experimental correlations of Motil et al.[3]

In the case of more viscous liquids under normal gravity, the model does not provide any useful predictions because the underlying frictional pressure drop correlation[6] was mostly validated for the air/water system.

Summary and Conclusions

The main contribution of this work is the development of a model based on two-phase volume-averaged equations for predicting the bubble to pulse transition in concurrent gas-liquid down flow through packed beds. To our knowledge, this is the first model able to predict flow regime transitions in packed beds across gravity levels. By recasting normal gravity correlations for the frictional pressure drop in a form similar to that of the correlation proposed by Motil et al.[2], we have shown that the presence of gravity leads to an increase of the frictional pressure drop (for concurrent down flow) under similar flow conditions. This in turn leads to a decrease in the liquid holdup with increasing gravity level. The model gives relatively good agreement with normal-gravity pressure drop and liquid holdup data in the bubble flow regime (air/water system). Also, linear stability analysis of the model leads to good quantitative agreement with data on the bubble-pulse flow regime transition for the air/water system, under both normal (down flow) and reduced (± 0.02 g) gravity. Reasonable agreement is also obtained for a wide range of liquid viscosities under reduced gravity conditions.

Acknowledgments

This work was supported by a grant from the NASA Glenn Research Center (Grant # NNX10AL37G). We thank Drs. Brian Motil and Enrique Ramé for helpful discussions.

Literature Cited

1. Patton MO, Bruzas AE, Rame E, Motil BJ. Development of the Packed Bed Reactor ISS Flight Experiment. 50th AIAA Aerospace Sciences Meeting. Nashville, TN; 2012.
2. Motil BJ, Balakotaiah V, Kamotani Y. Gas-liquid two-phase flow through packed beds in microgravity. *AIChE J*. 2003;49(3):557–565.
3. Motil BJ. *Fundamental Studies On Gas-Liquid Two-Phase Flows Through Packed Bed Reactors In Microgravity.* [PhD Dissertation] Case Western Reserve University; 2006.
4. Boelhouwer JG, Piepers HW, Drinkenburg AAH. Nature and characteristics of pulsing flow in packed bed reactors. *Chem Eng Sci*. 2002;57(22-23):4865–4876.
5. Benkrid K, Rode S, Pons MN, Pitiot P, Midoux N. Bubble flow mechanisms in trickle beds - an experimental study using image processing. *Chem Eng Sci*. 2002;57(16):3347–3358.
6. Rao VG, Ananth MS, Varma YBG. Hydrodynamics of two-phase cocurrent downflow through packed beds. Part II: experiment and correlations. *AIChE J*. 1983;29(3):467–483.
7. Sato Y, Hirose T, Takahashi F, Toda M. Pressure loss and liquid holdup in packed bed reactor with cocurrent gas-liquid downflow. *J Chem Eng Japn*. 1973;6(2):147–152.
8. Specchia V, Baldi G. Pressure drop and liquid holdup for two-phase concurrent flow in packed beds. *Chem Eng Sci*. 1977;52(5):515–523.
9. Sai PST, Varma YBG. Pressure drop in gas-liquid downflow through packed beds. *AIChE J*. 1987;33(12):2027–2036.
10. Ratnam GSV, Varma YBG. Effective interfacial area in gas-liquid cocurrent downflow through packed beds. *Bioprocess Eng*. 1991;7:29–34.
11. Anadon LD, Sederman AJ, Gladden LF. Mechanism of the trickle-to-pulse flow transition in fixed-bed reactors. *AIChE J*. 2006;52(4):1522–1532.
12. Ng KM. A Model for flow regime transitions in cocurrent downflow trickle-bed reactors. *AIChE J*. 1986;32(1):114–122.
13. Holub RA, Dudukovic' MP, Ramachadran PA. Pressure drop, liquid holdup, and flow regime transition in trickle flow. *AIChE J*. 1993;39(2):302–321.
14. Grosser K, Carbonell RG, and Sundaresan S. Onset of pulsing in two-phase cocurrent downflow through a packed bed. *AIChE J*. 1988;34(11):1850–1860.
15. Dankworth DC, Kevrekidis IG, Sundaresan S. Dynamics of pulsing flow in trickle beds. *AIChE J*. 1990;36(4):605–621.
16. Attou A, Ferschneider G. A Two-fluid hydrodynamic model for the transition between trickle and pulse flow in a cocurrent gas-liquid packed-bed reactor. *Chem Eng Sci*. 2000;55(3):491–511.
17. Wilhite BA, Blackwell B, Kacmar J, Varma A, McCready MJ. Origins of pulsing regime in cocurrent packed-bed flows. *Ind Eng Chem Res*. 2005;44(16):6056–6066.
18. Ishii M. *Thermo-Fluid Dynamic Theory of Two-Phase Flow,* Collection de la Direction des Etudes et Recherches d'Electricite de France. Paris: Eyrolles; 1975.
19. Lahey RT, Drew DA. The three-dimensional time and volume averaged conservation equations of two-phase flow. *Adv Nucl Sci Tech*. 1988;20:1–69.
20. Nigmatulin RI. Spatial averaging in the mechanics of heterogeneous and dispersed systems. *Int J Multiphase Flow*. 1979;5(5):353–385.
21. Nigmatulin RI, Lahey RT, Drew DA. On the different forms of momentum equations and on the intra- and interphase interaction in the hydromechanics of a monodispersed mixture. *Chem Eng Comm*. 1996;141-142:287–302.
22. Wild G, Larachi F, Charpentier JC. Heat and mass transfer in gas-liquid-solid fixed bed reactors. In: Quintard M, Todorovic M. *Heat*

and Mass Transfer in Porous Media. Amesterdam, The Netherlands: Elsevier; 1992:616–632.
23. Bordas ML, Cartellier A, Sechet P, Boyer Ch. Bubbly flow through fixed beds: microscale experiments in the dilute regime and modeling. *AIChE J*. 2006;52(11):3722–3743.
24. Attou A, Ferschneider G. A Simple model for pressure drop and liquid hold-up in packed-bed bubble reactors *Chem Eng Sci*. 1999; 54(21):5139–5144.
25. Khan A, Khan AA, Varma YBG. Flow regime identification and pressure drop in cocurrent gas-liquid upflow through packed beds. *Bioprocess Eng*. 1997;16:355–360.
26. Lamine AS, Colli Serrano MT, Wild G. Hydrodynamics and heat transfer in packed beds with cocurrent upflow. *Chem Eng Sci*. 1992; 47(13/14):3493–3500.
27. Turpin JL, Huntington RL. Prediction of pressure drop for two-phase, two-component concurrent flow in packed beds. *AIChE J*. 1967;13(6):1196–1202.
28. Tosun G. A Study of Cocurrent downflow of nonfoaming gas-liquid systems in a packed bed. 2. pressure drop: search for a correlation. *Ind. Eng. Chem. Process Des. Dev*. 1984;23(1):35–39.
29. Larachi F, Munteanu MC. Magnetic emulation of microgravity for earth-bound multiphase catalytic reactor studies - potentialities and limitations. *AIChE J*. 2009;55(5):1200–1216.
30. Triplett KA, Ghiaasiaan SM, Abdel-Khalik SI, Sadowski DL. Gas-liquid two-phase flow in microchannels - part i: two-phase flow patterns. *Int J Multiphase Flow* 1999;25:377–394.

Manuscript received July 3, 2013, and revision received Nov. 15, 2013.